Resonant perfect absorption of molybdenum disulfide beyond the bandgap

Hao Yu(于昊)[1], Ying Xie(谢颖)[1,†], Jiahui Wei(魏佳辉)[1], Peiqing Zhang(张培晴)[1], Zhiying Cui(崔志英)[2], and Haohai Yu(于浩海)[3]

[1] *Key Laboratory of Photoelectric Materials and Devices of Zhejiang Province, Ningbo University, Ningbo* 315211, *China*
[2] *Ningbo Yongxin Optics, Co., Ltd., Ningbo* 315211, *China*
[3] *State Key Laboratory of Crystal Materials and Institute of Crystal Materials, Shandong University, Jinan* 250100, *China*

(Received 8 May 2022; revised manuscript received 30 June 2022; accepted manuscript online 13 July 2022)

Light absorption and radiation are fundamental processes in optical science and engineering. Materials with perfect absorption properties play an important role in numerous optical applications. Following the meteoric rise of MoS_2 material, global opportunities and challenges coexist due to its extremely weak light–matter interaction capability beyond its energy band. In this work, we designed a kind of sandwich resonance structure and investigated MoS_2 as a perfect absorber in the infrared spectrum that should be transparent according to the optical band theory. The infrared absorption properties of W or Au/MoS_2/Au models at 800 nm–2400 nm were systematic simulated. By optimizing the structural parameters, the resonant wavelength of perfect absorption can be modulated from 830 nm to 1700 nm with angle insensitivity and polar independence. Moreover, we discovered that the bandwidth of absorption exceeding 50% of the W-top model reaches 500 nm, while that of the Au-top model is less than 100 nm, indicating that the top metal material has a great influence on the resonance absorption spectrum. Our work provides a practical route for enhancing and manipulating the light–matter interactions of low-dimensional materials beyond their own band gaps, which will be critical in the future design and implementation of optoelectronic devices and systems.

Keywords: multilayer MoS_2, Fabry–Perot structure, infrared absorption, resonance enhancement

PACS: 81.05.Xj, 02.70.Bf, 33.20.Ea, 42.79.Ta **DOI:** 10.1088/1674-1056/ac80ad

1. Introduction

Optical absorption is a fundamental process of light–matter interaction accompanied by amplitude attenuation and energy conversion.[1–4] Perfect absorption can be achieved by total amplitude modulation of the incident light and has promoted many functionalities and applications, including photovoltaics, radar cloaking and molecular detection.[5–10] For example, it has been shown that the analog of adding gain to achieve lasing was to add as much absorption as possible to the same structure with the corresponding lasing mode to be fully absorbed.[11] Applying materials with perfect absorption for fuselage design facilitates flight stealth radar and so on.[12] Traditional optical absorption materials are limited by optical selectivity and thickness, so studies on manipulating the amplitude state of excited electromagnetic waves have been ongoing for future high efficiency and integrated optical devices.

Recently, two-dimensional (2D) materials have sparked a research craze focusing on nano-optoelectronic fields, due to their tunable photonic band gap structures and excellent optical and electrical properties.[13–15] For most of these materials, the atoms are strongly bound by covalent bonds along in-plane directions and weakly held by van der Waals forces along out-of-plane directions. Such asymmetric forces make the absorption of polarized light in the parallel direction much stronger than in the vertical direction.[16] The feature of atomic layering inevitably leads to the problem of weak light–matter interactions. Recently, there have been many efforts to enhance the optical absorption of 2D materials, such as graphene, in a wide spectral range from to terahertz to visible frequencies.[17] Molybdenum disulfide (MoS_2), as a typical two-dimensional (2D) transition metal chalcogenide material, shows an optical band gap of 1.2 eV–1.8 eV[18] corresponding to the widest absorption band edge of the near-infrared (1 μm). Its optical absorption possesses a strong layer dependence since its optical sheet conductivity $\sigma(\hbar\omega)$ increases due to exciton absorption as the layer grows. Monolayer MoS_2 absorbs less than 8% of the incident light in the 400 nm–700 nm range;[19] moreover multilayer MoS_2 absorbs up to 60% of the incident light within its inherent visible range,[20] which far exceeds that of common 2D materials (e.g., monolayer graphene $\sim$ 2.3%, bilayer black phosphorus $\sim$ 15% with a negative layer dependence).[21–24] Many studies that have achieved visible perfect absorption of MoS_2 utilized metasurface-induced effects.[25–27] Utilizing plasmonic nanoantennas, the light absorption of MoS_2 was greatly enhanced and the photocurrent at 633 nm increased 10-fold.[28] An average absorption of 64.5% for monolayer MoS_2 was obtained in the visible range of 400 nm–750 nm using a tetramerized nanorod metasurface.[29] In other words, full-band or local-band high

[†]Corresponding author. E-mail: xieying@nbu.edu.cn

© 2023 Chinese Physical Society and IOP Publishing Ltd

absorption in the visible band has been realized.[30,31]

Nevertheless, multilayer MoS_2 material exhibits near transparency in the infrared region due to the intrinsic band limitation and frequency dispersion,[32] which hinders further infrared optoelectronic applications. In our previous works non-intrinsic infrared absorption was achieved by introducing Mo vacancies or S vacancies, from which passively *Q*-switched 1.42 μm laser generation using MoS_2 saturable absorbers, a mid-infrared 2717 nm MoS_2 photodetector and a mid-infrared 9.5 μm MoS_2 photodetector was obtained.[33–35] However, such absorption efficiency induced by band modulation is extremely low and it is difficult to satisfy the needs of practical applications in the infrared region. Enhancement of optical absorption of multilayer MoS_2 materials in the infrared band is still one of the key problems to be solved and there are relatively few studies on this. Realization of tunable high optical absorption of MoS_2 in the infrared band, based on Fabry–Perot (FP) resonance theory,[36] would be an important achievement.

In this work, we designed a structure consisting of a MoS_2 layer sandwiched between layers of dielectric metal *X* (X = W, Au, Ni, Cr, Nb, Pd) and numerically simulated the resonant broadband absorption from 800 nm to 2400 nm beyond its band gap. With changing the working metal material and thickness, the infrared optical absorptance was greatly enhanced by up to 100% at the resonance wavelength, which means actual perfect absorption was achieved defying the limitation of the MoS_2 band gap. The resonance wavelength with perfect absorption properties can be tuned from 830 nm to 1700 nm with angle insensitivity and polarization independence. This structure can be easily fabricated and integrated with other photoelectric materials and elements and optoelectronic devices, and should have promising applications in future multifunctional optoelectronic devices.

2. Model and mechanism

2.1. Simulation model

Figure 1 shows a three-dimensional structure diagram of the W/MoS_2/Au structure, where d_1, d_2, and d_3 are the thicknesses of the W, MoS_2 and Au layers, respectively. A SiO_2 wafer was prepared as the base of the structure, on which a layer of Au was added as an anti-penetration layer. The optical absorbing media MoS_2 and W were directly coated on top of the Au layer. The commercial finite-difference time-domain (FDTD) software (Lumeric Solutions, Inc.) was used for simulation and the applied optical parameters were taken from the refractive index database. In the simulation model, the perfect matching layer (PML) was used as the boundary condition in the *z* direction. Since all films used in the simulation were assumed to be isotropic, periodic boundary conditions were set in the *x* and *y* directions. The light source was set as an omnidirectional plane electromagnetic wave with perpendicular incidence, placed on top of the film. The amplitude of the electric field was set to 1.0 V·m^{-1}. A 2D optical power monitor was placed between the light source and the upper boundary of the PML to obtain the reflection of the designed structure. A 2D field monitor was used to obtain the electric field distribution in each layer of the structure.

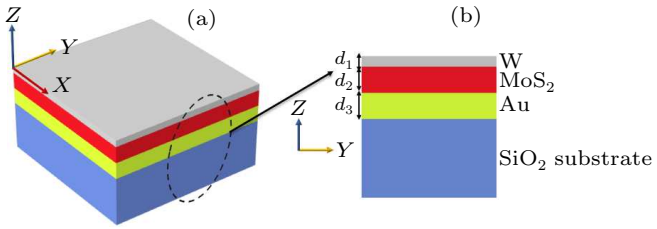


Fig. 1. Schematic diagram of the MoS_2-based sandwich Fabry–Perot structure with dimensions specified.

2.2. Mechanism of absorption enhancement

For comparison, the optical absorption properties in the range of 800 nm–2400 nm for monolayer and bilayer models were also studied. In the three different models d_1 was set to 10 nm, d_2 was set to 60 nm and d_3 was set to 100 nm. As shown in Fig. 2(a), the intrinsic MoS_2 film is nearly transparent when the wavelength exceeds 1 μm, corresponding well to a bandgap of 1.2 eV. This also shows that our calculation method is reasonable and the results are reliable. A similar absorption spectrum induced by a W–MoS_2 structure reveals the negligible role of an individual W layer. In contrast, the absorptance of a MoS_2–Au structure was more than 50% at 1250 nm since the high reflection of the Au layer reduced the transmission loss of light and increased the interaction time of light on the absorption layer. The effect of the thickness of the bottom Au layer (d_3) on the absorption performance of the MoS_2–Au structure is shown in Fig. S1. As the thickness d_3 increases from 30 nm to 100 nm the absorption does not continue to improve, which shows that the enhancement of the absorption performance of the bilayer MoS_2–Au structure is limited. Therefore, only through functional integration could the W/MoS_2/Au structure model could achieve a broad high absorption bandwidth of 1100 nm–1700 nm and completely absorb light with a wavelength of 1350 nm. We observed a red shift of approximately 93 nm in the three-layer structure which may be caused by a slight phase shift of light passing through the top metal layer. These results indicate the need for each layer and their synergistic effects for achieving high absorption of multilayer MoS_2 in the infrared band.

To verify the accuracy and reliability of the above analysis obtained by FDTD simulation, COMSOL Multiphysics simulation was applied to the same designed structure. As shown in Fig. 2(b), the peak of almost complete absorption is located at 1340 nm, which agrees well with the result (1350 nm) from

FDTD simulation. Meanwhile, the electric field distribution over the cross section of the FP structure was simulated, as shown in Fig. 2(c). Most notably, most of the energy of the incident light was trapped in the middle MoS_2 layer, and the bottom Au layer effectively blocked incident light from entering the SiO_2 base.

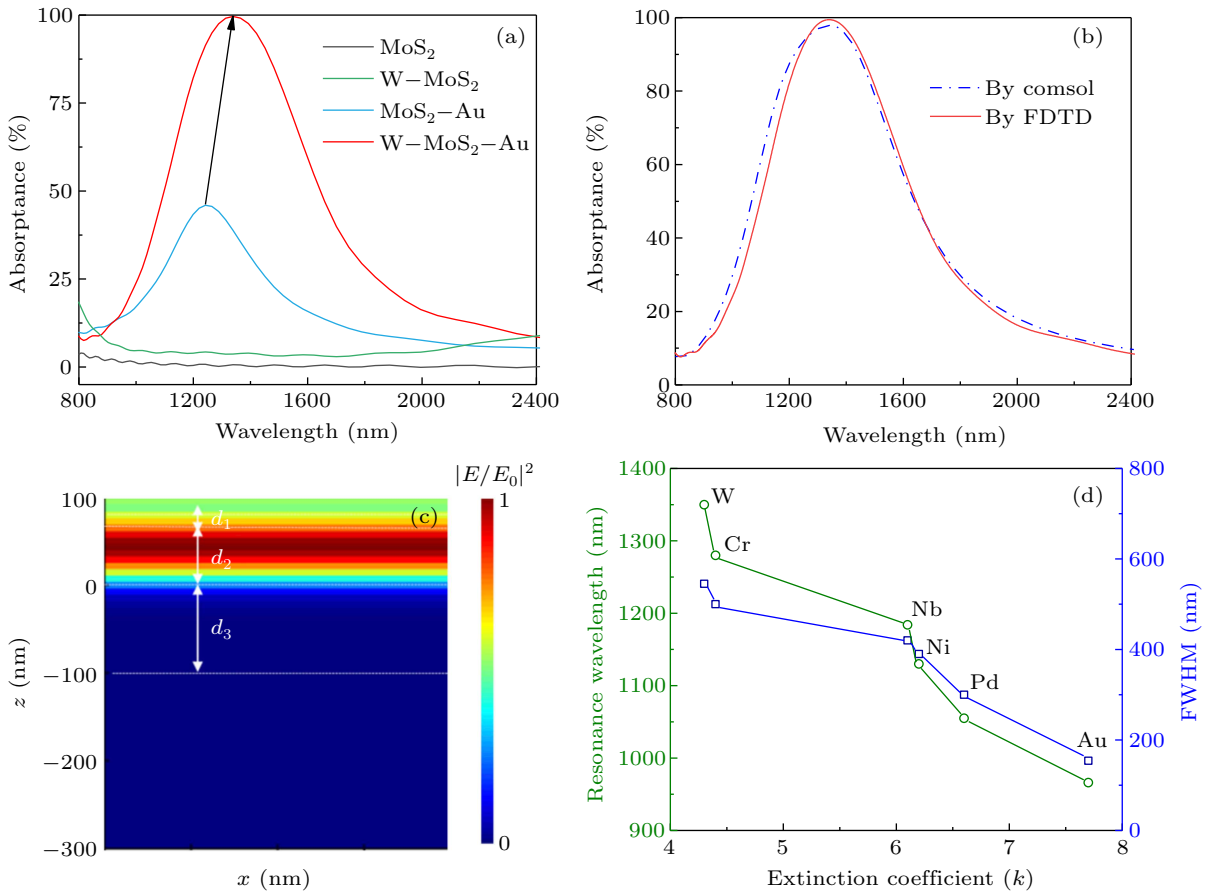


Fig. 2. (a) Absorption spectra for a W/MoS_2/Au structure calculated using the FDTD method: only middle and bottom layers, only top and middle layers, three layers. (b) Absorption of designed MoS_2-based sandwich FP structure using FDTD simulation and COMSOL Multiphysics simulation under illumination of normal incident light. (c) Electric field distribution over the cross-section of the W/MoS_2/Au structure at 1335 nm. (d) The relationship among the extinction coefficients (k) of different top metals (W/Cr/Nb/Ni/Pd/Au), FWHM and resonant wavelength when the FP cavity structure achieves perfect absorption.

In fact, the high absorption efficiency was mainly due to the FP cavity resonance of the W/MoS_2/Au structure.[37,38] The reflection R can be described as[39]

$$R = \frac{2\sqrt{R_1R_2}(1-\cos\delta)}{\left(1+R_1R_2-\sqrt{R_1R_2}\cos\delta\right)}, \tag{1}$$

where R_1 and R_2 represent the intensity of reflectivity corresponding to the top W–MoS_2 and bottom Au–MoS_2 interfaces, respectively. The total phase shift accumulated in one round trip in the cavity is expressed as[40]

$$\delta = \Phi_{\text{prop}} - (\Phi_1 + \Phi_2), \tag{2}$$

where Φ_1 and Φ_2 denote the reflection phase shifts associated with the metal–dielectric interfaces. The round-trip propagation phase shift for the normal incidence is calculated as

$$\Phi_{\text{prop}} = 4\pi nd/\lambda, \tag{3}$$

where n and d are the refractive index and cavity thickness, respectively. The absorption A can be calculated using $A = 1 - T - R$, considering that transmission T is negligible as a result of the strong Au layer. The reflection is said to be minimum at the resonance wavelength, where the condition $\delta = 2m\pi$ ($m = 0, 1, 2, \ldots$) is satisfied.[41] Meanwhile, the absorption of the sandwich structure reaches its maximum.

Next, we studied the effect of the top metal material on the absorption spectra. The thickness of the middle MoS_2 (d_2) was set to 60 nm, and the thickness of the top metal (d_1) was set to 10 nm. We fabricated FP structures with W, Cr, Ni, Nd, Pd, and Au, respectively, and investigated the resonant absorption properties (see Fig. S2). The results show that the resonant wavelengths were located in the infrared band, which indicates that all the structures have the potential to enhance the infrared light–matter interactions of multilayer MoS_2. The full width at half maximum (FWHM) of the absorption response can be defined as a standard for judging the bandwidth of enhanced high absorption. As shown in Fig. 2(d), the FWHMs of the designed FP structures show an obvious dependence on the type

of top metal material. This could be because the extinction coefficients (k) of the metal materials were inversely proportional to the intensity of the incident light passing through the metal layer (see Fig. S3). As the resonances appeared, the smaller the k was the greater the amount energy that entered, therefore the spectral response was broader. We noted that the resonant wavelength shifts in the designed structures consisting of different top materials; this could be because the metals have their own penetration depth, thus leading to varied effective optical path lengths. Based on the above simulation results, we finally selected W and Au as the top metal materials for further research as they have the widest and narrowest FWHM, respectively.

3. Results and discussion

3.1. A thin-film resonant structure based on W

According to the above theory, we know that the absorption properties of designed sandwich FP structures are inseparable from the material and thickness. We first compared the reflectivity of the three bottom metals (Ag, Au, and Al) in the range 800 nm–400 nm (see Fig. S4(a)), and the results show that their reflectivities are almost the same (all above 95%). The effect of different bottom metals (Ag, Au, and Al) on the absorption of the FP structure is shown in Fig. S4(b); the results show that all the above bottom metal layers can achieve high resonance absorption in the structure, but the resonance position shows a slight change. Therefore, we finally chose Au as the bottom layer for the simulations. As shown in Fig. 3(a), the thickness of the bottom Au film was set to 100 nm to ensure that no light could pass through, thus providing a strong reflection. The refractive indices and extinction coefficients of Au, MoS_2, and W are shown in Fig. 3(b). As the results suggest, MoS_2 acts as a lossless dielectric material in the infrared range. For W metal, the curves of the refractive index and extinction coefficient crossed at 1700 nm, close to the bulk plasma frequency at which the intrinsic absorption occurs.

In order to investigate the effect of W-layer thickness on absorption enhancement, the evolution of structural absorption depending on W-layer thickness was simulated. The thickness of the MoS_2 layer was set to 100 nm. As shown in Fig. 3(c), when the W-layer thickness increases, the resonance wavelength shows a clear blue shift. The deviation of the resonance wavelength between 5 nm thick W and 15 nm thick W is near 120 nm. This may be caused by a slight phase shift of light passing through the W layer. In addition, when the W-layer thickness is more or less than 15 nm, the absorption peak will decline. This may be because the thicker film means that less light enters the structure, or the thinner film cannot form a FP cavity. So, according to Fig. 3(d), the W-layer thickness is set to 7 nm–17 nm to form an effective sandwich FP structure and obtain the optimal effect of absorption enhancement.

When the thicknesses of the top W film and bottom Au film are fixed, the structural absorption characteristics are only determined by the MoS_2 thickness. Figure 3(e) shows the evolution of the absorption spectrum as the MoS_2 layer thickens. When the thickness of the MoS_2 layer increases from 30 nm to 100 nm, a red shift occurs in the high absorption peak from 900 nm to 1700 nm. Meanwhile, the FWHM of the enhanced absorption curve is near to 500 nm. As shown in Fig. 3(f), the near-linear deep red band extends from 900 nm to 1700 nm. The deep red band means high absorption ($\sim 99\%$) of the FP structure, and also represents extremely low reflection. This result indicates that continuous wide band tuning could be manipulated by simply changing the thickness of the MoS_2 layer in the W/MoS_2/Au structure.

We then investigated the spectral stability as the incident angle changes. A 2D plot of the reflectance versus angle and wavelength is depicted in Fig. 4. When the incident angle increases from 0° to 50°, the deep blue band gradually shifts. The blue band in different polarization states of the incident light shows similar behavior. The reason for the slight blue shift is that with the increase in the incident angle, the phase delay within the W–MoS_2 interface at the shorter wavelength was more than that at the longer wavelength. The result shows angle insensitivity (less than 50°) and polarization independence of the W/MoS_2/Au structure to incident light.

3.2. A thin-film resonant structure based on Au

We compared the absorption characteristics of W-based and Au-based FP structures. After the same structural optimization, the thickness of the top Au layer was set to 5 nm–10 nm to induce optimal absorption. For the Au/MoS_2/Au structure we found an interesting phenomenon different from the W/MoS_2/Au structure. As shown in Fig. 5(a), the high absorption peak has a red shift from 830 nm to 1300 nm as the MoS_2 layer thickness increases from 30 nm to 90 nm. The FWHM of the absorption curve is near to 100 nm. Therefore, the Au-based FP structure can only maintain high absorption in a narrow band. As shown in Fig. 5(b), the deep red band is not as continuous as that of the W-based FP cavity structure but scatters in a small region. This result indicates that a high-absorptivity narrow band can be tuned continuously by manipulating the thickness of the MoS_2 layer in the Au/MoS_2/Au structure.

Spectral stability as the incident angle increases was also simulated. As shown in Fig. 6, similar to the analysis above, the deep blue band in different polarization states shifts slightly. The results show that the Au/MoS_2/Au structure is insensitive to angle and polarization of the incident light.

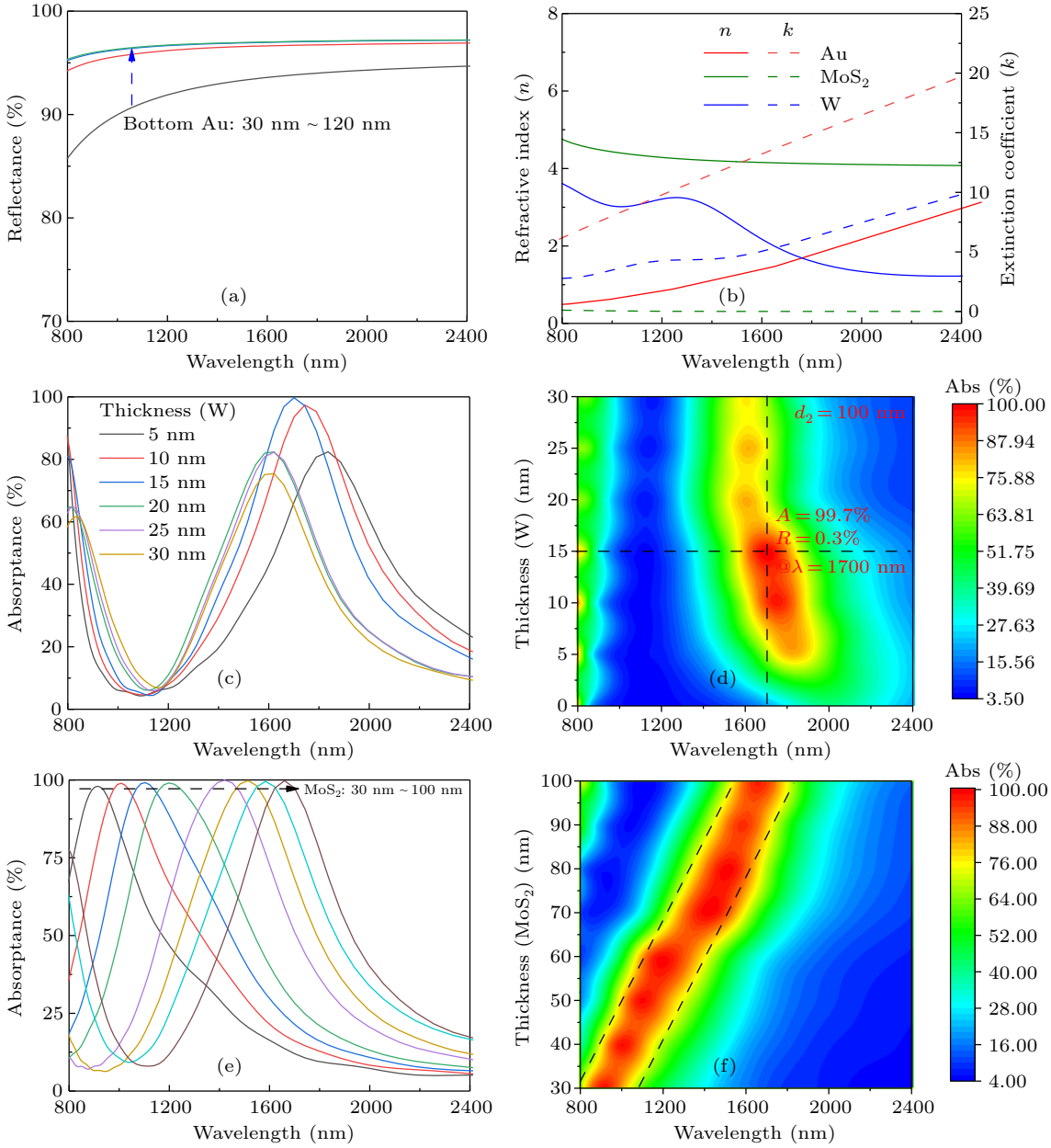


Fig. 3. (a) The evolution of reflectance as the thickness of the bottom Au layer increases from 30 nm to 120 nm. (b) The refractive indices and extinction coefficients of Au, MoS_2, and W. The solid lines represent the refractive index and the short dashed lines show the extinction coefficient. (c) The comparison of absorption spectra with top W films of 5 nm, 10 nm, 15 nm, 20 nm, 25 nm, and 30 nm. (d) 2D plot of absorptance versus wavelength and the thickness of W. The reflection dip and absorption peak occur at the resonance wavelength. (e) Comparison of absorption spectra with MoS_2 films of 30 nm, 40 nm, 50 nm, 60 nm, 70 nm, 80 nm, 90 nm, and 100 nm. (f) 2D plot of absorptance versus wavelength and the thickness of MoS_2. An extension of the deep red band denotes a red shift of absorption peak as the thickness of MoS_2 increased.

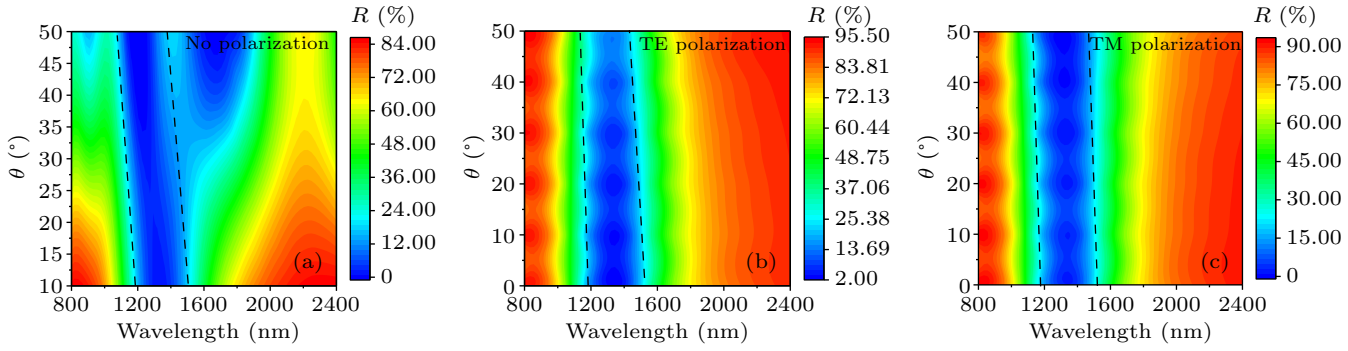


Fig. 4. The evolution of reflectance as the incident angle increases. $d_1 = 7$ nm, $d_2 = 60$ nm: (a) no polarization, (b) TE polarization and (c) TM polarization represent three kinds of light. TM polarization: there is an electric field component but no magnetic field component in the propagation direction; called a transverse magnetic wave. TE polarization: there is a magnetic field component but no electric field component in the direction of propagation; called a transverse electric wave.

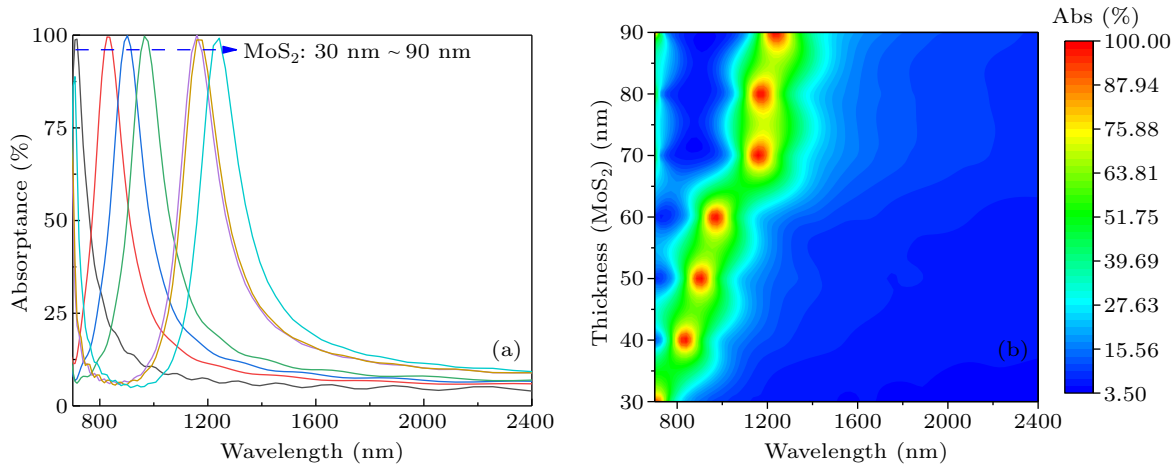


Fig. 5. (a) Comparison of absorption spectra with MoS_2 films of thickness 30 nm, 40 nm, 50 nm, 60 nm, 70 nm, 80 nm, and 90 nm. (b) 2D-plot of absorptance versus wavelength and the thickness of MoS_2. An extension of the deep red band denotes a red shift of absorption peak as the thickness of MoS_2 increases.

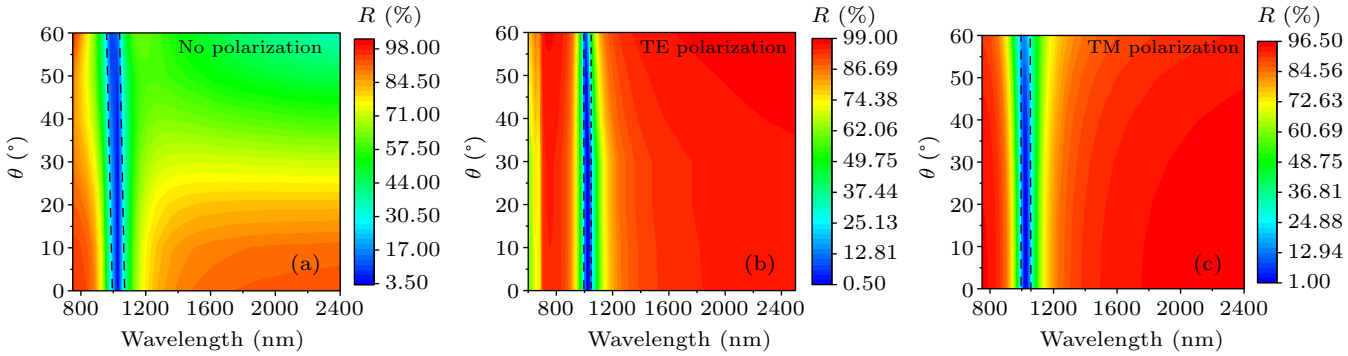


Fig. 6. The evolution of reflectance as the incident angle increases. $d_1 = 8$ nm, $d_2 = 70$ nm. (a) No polarization, (b) TE polarization, and (c) TM polarization represent three kinds of light.

4. Conclusion

In summary, a MoS_2-based sandwich resonant structure was designed and the infrared absorption characteristics beyond its band gap were investigated by the FDTD method. The results reveal that the FP resonance effectively modulates the light–matter interactions and that perfect absorption of multilayer MoS_2 was achieved beyond its inherent band gap. By changing the thickness of the MoS_2 layer, the perfect absorption wavelength can be tuned continuously from 900 nm to 1700 nm in the W/MoS_2/Au structure and 830 nm to 1300 nm in the Au/MoS_2/Au structure. The bandwidth of the high absorption region (more than 50%) can be modulated from near 100 nm to 500 nm. Furthermore, the infrared absorption properties of the designed sandwich structures show angle insensitivity (less than 60°) and polar independence of the incident light. Our work focuses on the enhancement of optical absorption properties of MoS_2 outside the scope of optical energy transition and provides a practical route. We believe this is very important for exploring the promising light–matter interactions of 2D materials and should broaden some potential infrared applications in the broadband or wavelength-selective photoelectric fields.

Acknowledgments

Project supported by the National Natural Science Foundation of China (Grant No. 62105169), Natural Science Foundation of Ningbo (Grant No. 2021J078), and Special fund for Talents Project of Ningbo University (Grant No. 432094940).

References

[1] Qin M, Wang L, Zhai X, Chen D and Xia S 2017 *Nanoscale Res. Lett.* **12** 1
[2] Splendiani A, Sun L, Zhang Y, Li T, Kim J, Chim C Y, Galli G and Wang F 2010 *Nano Lett.* **10** 1271
[3] Zhao Z, Wang D, Gao H, Yang Z, Cao H and He W 2019 *Dyes Pigment.* **164** 182
[4] McKagan S, Handley W, Perkins K and Wieman C 2009 *Am. J. Phys.* **77** 87
[5] Fournier D, Boccara C, Skumanich A and Amer N M 1986 *J. Appl. Phys.* **59** 787
[6] Balucinska-Church M and McCammon D 1992 *Astrophys. J.* **400** 699
[7] Klassen S 2011 *Sci. Educ.* **20** 719
[8] Long M, Wang P, Fang H and Hu W 2019 *Adv. Funct. Mater.* **29** 1803807
[9] Miao J and Zhang F 2019 *J. Mater. Chem. C.* **7** 1741
[10] Fang H and Hu W 2017 *Adv. Sci.* **4** 1700323
[11] Wang C, Sweeney W R, Stone A D and Yang L 2021 *Science* **373** 1261
[12] He H, Shang X, Xu L, Zhao J, Cai W, Wang J, Zhao C and Wang L 2020 *Opt. Express* **28** 4563
[13] Xia F, Wang H, Xiao D, Dubey M and Ramasubramaniam A 2014 *Nat. Photonics* **8** 899

[14] Manzeli S, Ovchinnikov D, Pasquier D, Yazyev O V and Kis A 2017 *Nat. Rev. Mater.* **2** 17033
[15] Mas-Balleste R, Gomez-Navarro C, Gomez-Herrero J and Zamora F 2011 *Nanoscale* **3** 20
[16] Tan D, Lim H E, Wang F, Mohamed N B, Mouri S, Zhang W, Miyauchi Y, Ohfuchi M and Matsuda K 2017 *Nano Research* **10** 546
[17] Yan Z, Zhu Q, Wan M, Lu X, Pu X, Tang C and Yu L 2020 *Opt. Express* **28** 6095
[18] Li X and Zhu H 2015 *J. Materiomics* **1** 33
[19] Bernardi M, Palummo M and Grossman J C 2013 *Nano Lett.* **13** 3664
[20] Wang K, Wang J, Fan, Lotya M, O'Neill A, Fox D, Feng Y, Zhang X, Jiang B and Zhao Q 2013 *ACS Nano* **7** 9260
[21] Qing Y M, Ma H F, Ren Y Z, Yu S and Cui T J 2019 *Opt. Express* **27** 5253
[22] Xiao S, Wang T, Liu Y, Xu C, Han X and Yan X 2016 *Phys. Chem. Chem.* **18** 26661
[23] Cai Y, Xu K D, Feng N, Guo R, Lin and Zhu J 2019 *Opt. Express* **27** 3101
[24] Qing Y M, Ma H F and Cui T J 2018 *Opt. Express* **26** 32442
[25] Robertson K W, Lota LaPierre R and Lota Krich J 2019 *Opt. Express* **27** A133
[26] Uddin M J and Magnusson R 2013 *Opt. Express* **21** 12495
[27] Miyata M, Hatada H and Takahara J 2016 *Nano Lett.* **16** 3166
[28] Britnell L, Ribeiro R M, Eckmann A, Jalil R, Belle B D, Mishchenko A, Kim Y J, Gorbachev R V, Georgiou T and Morozov S V 2013 *Science* **340** 1311
[29] Pei Y, Sang T, Mi Q, Wang J and Wang Y 2021 *J. Opt.* **24** 024001
[30] Long L, Yang Y, Ye H and Wang L 2017 *J. Quant. Spectrosc. Radiat. Transf.* **200** 198
[31] Cheng Z Q, Luo X, Xu L, Zhai X and Wang L L 2020 *Opt. Express* **28** 14151
[32] Wang W, Klots A, Prasai D, Yang Y, Bolotin K I and Valentine J 2015 *Nano Lett.* **15** 7440
[33] Xie Y, Liang F, Wang D, Chi S, Yu H, Lin Z, Zhang H, Chen Y, Wang J and Wu Y 2018 *Adv. Mater.* **30** 1804858
[34] Xie Y, Zhang B, Wang S, Wang D, Wang A, Wang Z, Yu H, Zhang H, Chen Y and Zhao M 2017 *Adv. Mater.* **29** 1605972
[35] Wang, Yu H, Zhang H, Wang A, Zhao M, Chen Y, Mei L and Wang J 2014 *Adv. Mater.* **26** 3538
[36] Yao Y, Liao Z, Liu Z, Liu X, Zhou, Liu G, Yi Z and Wang J 2021 *J. Phys. D: Appl. Phys.* **54** 113002
[37] Shu, Li Z and Xia Li Y 2013 *Opt. Express* **21** 25307
[38] Huang W X, Zhao G R, Guo J J, Wang M S and Shi J P 2016 *Chin. Phys. Lett.* **33** 088103
[39] Park C S and Lee S S 2021 *ACS Appl. Nano Mater.* **4** 4216
[40] Tan J, Wu Z, Xu K, Meng Y, Jin G, Wang L and Wang Y 2020 *Plasmonics* **15** 293
[41] Barnes W L 2006 *J. Opt. A: Pure Appl. Opt.* **8** S87